DYNAMIC STRAIN MAPPING AND REAL-TIME DAMAGE STATE ESTIMATION UNDER BIAXIAL RANDOM FATIGUE LOADING

SUBHASISH MOHANTY*, ADITI CHATTOPADHYAY*, JOHN N. RAJADAS**, AND CLYDE COELHO*

ABSTRACT. Fatigue damage and its prediction is one of the foremost concerns of structural integrity research community. The current research in structural health monitoring (SHM) is to provide continuous (or on demand) information about the state of a structure. The SHM system can be based on either active or passive sensor measurements. Though the current research on ultrasonic wave propagation based active sensing approach has the potential to estimate very small damage, it has severe drawbacks in terms of low sensing radius and external power requirements. To alleviate these disadvantages passive sensing based SHM techniques can be used. Currently, few efforts have been made towards, time-series fatigue damage state estimation over the entire fatigue life (stage-I, II & III). A majority of the available literature on passive sensing SHM techniques demonstrates the clear trend in damage growth during the final failure regime (stage-III regime) or during when the damage is comparatively large enough. The present paper proposes a passive sensing technique that demonstrates a clear trend in damage growth almost over the entire stage-II and III damage growth regime. A strain gauge measurement based passive SHM frameworks that can estimate the time-series fatigue damage state under random loading is proposed. For this purpose, a Bayesian Gaussian process nonlinear dynamic model is developed to map the reference condition dynamic strain at a given instant of time. The predicted strains are compared with the actual sensor measurements to estimate the corresponding error signals. The error signals estimated at two different locations are correlated to estimate the corresponding fatigue damage state. The approach is demonstrated for an Al-2434 complex cruciform structure applied with biaxial random loading.

NOMENCLATURE

a^n n^{th} damage level damage index

d^n n^{th} damage level damage value

ΔN Number of fatigue cycles between two adjacent damage level

g^n n^{th} damage level nonlinear function with respect to hidden state x

h^n n^{th} damage level nonlinear function with respect to strain measurements u or y

$H_{U \to u}$ Transfer function between environmental load U and input strain u

$H_{U \to y}$ Transfer function between environmental load U and output strain y

m Time lag coefficient in sensor observation at n^{th} damage level

n (Superscripts) Symbolizes discrete damage level

u Input strain at location 1

U Environmental load

x^n n^{th} damage level hidden state

y Output strain at location 2

ϵ_i Strain at location i

0 (Superscripts) Symbolizes reference or healthy condition

*Mechanical and Aerospace Engineering, Arizona State University, Tempe, AZ, 85287, USA, smohant2@asu.edu, aditi@asu.edu, Clyde.Coelho@asu.edu

**Engineering Technology Department, Arizona State University Polytechnic, Mesa, AZ, 85212, USA, rajadas@asu.edu.

1. Introduction

Real-time structural health monitoring (SHM) is an emerging research area with multiple applications in aircraft structures. The design and operation of civil and military aircraft require a strict regiment of inspection and maintenance based on damage tolerant [6] principles, that ensures the operational safety from the structural point of view. The inspection and maintenance cost typically constitutes approximately 30-40 percent of any individual aircraft's total life cycle cost. The current research on structural health monitoring [2, 7, 20] can lead to lower inspection and maintenance cost and reduces the long overhauling time for maintenance. Currently there are two different SHM techniques based on active and passive sensing approaches. For an active sensing based SHM technique, a fixed input signal is introduced to the host structure using an actuator. The corresponding sensor signals are analyzed to interrogate the presence of damage in the structure and to estimate its extent and severity of damage. The passive SHM infers the state of the structure using passive sensor signals that are monitored over time. Currently there is a sizeable amount of research being conducted on active sensing based damage interrogation techniques [1, 10, 14, 15, 18]. These techniques are related to narrowband wave propagation based pitch-catch, pulse-echo, phased array structural radar approaches. Also research has been initiated in the area of time-series fatigue damage state estimation [5, 10, 11]. To estimate fatigue damage, continuous monitoring of the structure is required over its entire fatigue life. Recently Mohanty et al [12] proposed an unsupervised broadband active sensing technique, which can estimate sub-millimeter level damage over the entire fatigue life, including stage-I, II and III crack growth regime. The technique was effectively used to monitor critical structural hot-spots such as lug-joints that connect the fuselage with the main wing box. It must be noted that although the active wave propagation based interrogation technique can estimate very small damage, it has a few drawbacks. The sensing radius of an individual active sensing node is very small (of the order of centimeters), thus requiring a large number of actuators and sensors to monitor a large structure. The need for large number of sensors can limit the usability of active sensing approach in large structures such as aircraft wing. Also the wave based techniques require an external excitation source, which limits their applications. Keeping in mind both the advantages and disadvantages of active sensing techniques, it is practical to use active wave based techniques in highly sensitive and localized hotspot, whereas the rest of the structure can be monitored using passive sensing [3, 19]. The passive sensing technique has some advantages over active wave based techniques. For example passive techniques are more global and can monitor large structures if sensors are placed strategically. In addition, passive sensing techniques do not require any external power source. Though the use of different types of passive sensors is application specific, the accelerometer based damage monitoring approaches [8, 16, 22] are less sensitive to detect incipient smaller damage, which can lead to the estimated damage signatures become prominent only during the final failure regime. To alleviate the disadvantages of both wave based active sensing and accelerometer based passive sensing approaches, a novel strain gauge measurements based passive damage interrogations technique is used in the present paper. Though the strain gauge measurement is more local to accelerometer measurement, it is more global to wave based active sensing techniques. The strain gauges can be placed strategically in structural hot-spots for passive and continuous monitoring of fatigue damage. It is to be noted that the strain gauge sensing techniques are more mature compared to wave based active sensing techniques. They do not require any external power source. Recently Mohanty and et al [11] have demonstrated the use of strain gauges for real-time and time-series damage state estimation of an Al-6061 cruciform specimen under biaxial constant amplitude fatigue loading. However, damage estimation under random loading is more complicated compared to damage interrogations under constant amplitude fatigue loading. The present paper discusses a novel strain gauge measurement based passive sensing technique that can estimate time-series damage states under random loading. The approach is demonstrated for an Al-2024 cruciform specimen subjected to biaxial random loading.

2. Theoretical Approach

Structural systems such as an aircraft in flight undergo random loading. Different locations of the structure may experience different strain fields. There exists a particular correlation pattern between the dynamic strain fields measured at those locations, which may change due to damage. The change in correlation pattern can be mapped as a time-varying transfer function which can be a measure of time-varying damage condition. A schematic of the nth damage level transfer function (H^n) between dynamic strains at two points is shown in Figure (1). The dynamic strain at location 1 i.e., ϵ_1 can be considered as input u, whereas the dynamics strain at location 2 i.e., ϵ_2 can be considered as output for the estimation of H^n. Note that the strain at both the locations are function of the environmental load U and the damage condition of the structure at that time. Structural fatigue damage condition can be monitored in real-time by acquiring real-time signals from passive sensors such as strain gauges. By using the strain measurements at two different locations, the damage state of the structure between those two points can be estimated. To estimate the time-series damage states, the over all fatigue damage process can be divided into multiple short term discrete instances (Figure 2). For constant cycle fatigue loading, these discrete damage states can be estimated by directly correlating the corresponding dynamic strains measured at different locations, which has already been demonstrated by Mohanty and et al. [11]. However, for random loading, estimation of time-series damage states is more complicated, due to the variation in the strain correlation (between two points) pattern with varying loads. That means it is not possible to directly identify whether the correlation pattern change is due to change in load or due to damage. It should be noted that in the work reported by Mohanty and et al. [11] the load information was not included in the damage index formulation. For accurate damage state estimation under random loads, the loading information should be included in the damage index formulation. In addition to the loading information, other time varying input parameters such as temperature and humidity can also be included in the damage index formulation. Details of the damage index formulation are discussed in the following sections.
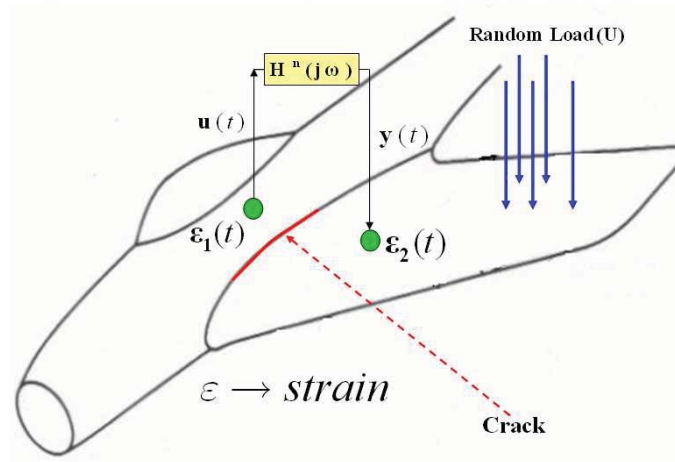

FIGURE 1. Schematic showing strain at two points of a structure and the time-varying transfer function between them.

2.1. **Dynamic model estimation.** One of the major steps in the proposed time-series damage state estimation approach is to estimate the nonlinear dynamic model using strain gauge and environmental load measurements. Two models have to be estimated one between environmental loading
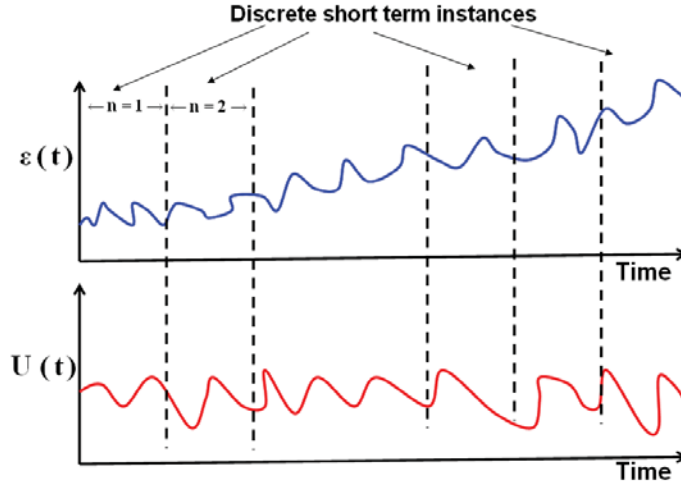
FIGURE 2. Schematic showing the division of overall fatigue life to multiple discrete short term instances.

U and input strain $u(= \epsilon_1)$ at location 1 and the other between environmental loading U and output strain $y(= \epsilon_2)$ at location 2. The following sections describe the procedure for dynamic model estimation.

2.1.1. *Generic nonlinear dynamic model.* Assume that the nth damage level can be described by sensor signals acquired between $n = N$ and $n = N + \Delta N$ fatigue cycle, where ΔN is the interval in fatigue cycles between which the damage state has to be estimated. It is assumed that during $n = N$ to $n = N + \Delta N$ fatigue cycle, the damage condition of the structure remains unchanged. The sensor measurements between $n = N$ and $n = N + \Delta N$ fatigue cycles are indexed by $m = 0, 1, \ldots, M$. The nth damage level nonlinear dynamic model [23] between environmental input $U^n(m) = \{L^n(m), T^n(m), H^n(m)\}$ and input strain $u^n(= \epsilon_1)$ at location 1 can be expressed as

$$\text{(1)} \qquad x^n(m) \;=\; g_u^n(x^n(m-1), U^n(m), d^n)$$
$$\text{(2)} \qquad u^n(m) \;=\; h_u^n(x^n(m), U^n(m), d^n)$$

Similarly the nth damage level nonlinear dynamic model between environmental input $U^n(m)$ and output strain $y^n(= \epsilon_y)$ at location 2 can be expressed as

$$\text{(3)} \qquad x^n(m) \;=\; g_y^n(x^n(m-1), U^n(m), d^n)$$
$$\text{(4)} \qquad y^n(m) \;=\; h_y^n(x^n(m), U^n(m), d^n)$$

where the superscript n represents the nth damage level, $x^n(\cdot)$ represents the nth damage level hidden states, d^n is the quantitative value of damage condition at n^{th} damage level, $U^n(m) = \{L^n(m), T^n(m), H^n(m)\}$ represents the input environmental conditions with $L^n(m), T^n(m)$ and $H^n(m)$, represent the nth damage level load, temperature and humidity, respectively, with lag coefficient m. $L^n(m)$ is a vector with input from multiple loading sources. In addition $g_{(\cdot)}^n$ and $h_{(\cdot)}^n$ are two nonlinear mapping functions. In the present work with laboratory test condition there is not much change in temperature and humidity. Because of this in numerical validation of the developed techniques the temperature and humidity variables will not considered. However, for generality temperature and humidity variables are included in the discussed theoretical formulation. It is also to be noted that in the present formulation time is not explicitly considered as an input

variable. However, for time dependant degradation cases such as in case of creep damage, time has to be considered as additional input parameter. For example with applied mechanical and thermal load the input variable can be represented as $U^n(m) = \{L^n(m), T^n(m), H^n(m), n\}$. Again to note that, in the present formulation it is assumed that during $n = N$ to $n = N + \Delta N$ fatigue cycle, the damage condition of the structure remains unchanged. If time dependant creep damage has also to be considered between $n = N$ and $n = N + \Delta N$ fatigue cycles the input variable can be further modified as $U^n(m) = \{L^n(m), T^n(m), H^n(m), n(m)\}$.

2.1.2. *Nonlinear dynamic modeling using Bayesian Gaussian Process.* Nonlinear dynamic modeling and signal processing have been gaining increased interest from researchers in recent years. Numerous researchers have contributed to the development and increased understanding of these fields [13]. Examples of different nonlinear models are with smooth nonlinearities, multiple-values nonlinearities, (e.g., hysteresis), non-smooth nonlinearities with discontinuities. The smooth nonlinearities can be represented by polynomial models. To describe a polynomial nonlinear system, the Volterra expansion has been the most widely used model for the last thirty years. The continuous-time Volterra filter model is based on Volterra series expansion. However the Volterra kernel nonlinear model is computationally intensive for highly nonlinear systems. In addition, polynomial type Volterra methods are more suitable to model smooth nonlinearity. However fatigue damage consists of multiple-valued nonlinearities, e.g., hysteresis effect, in stress-strain relation and requires a better robust approach to model it. The Bayesian Gaussian Process (GP) model [4, 9, 17] can be useful for modeling the nonlinear dynamics associated with the individual discrete damage instances. Using GP based high-dimensional kernel transformation, the nonlinear relation between the input environmental loading $U^n(m) = \{L^n(m), T^n(m), H^n(m)\}$ and the input/output strain (i.e $u^n(= \epsilon_1)$ or $y^n(= \epsilon_2)$ can first be mapped in a high-dimensional space. The high-dimensional transformation is performed using assumed kernel functions [4, 9, 17]. It is assumed that in the transformed high-dimensional space the input environmental load and the input/output strain follow a linear relation. In the high-dimensional space the mapping between the new transformed input $X = \Phi(U^n(m)))$ and observed input/output strain (i.e $u^n(= \epsilon_1)$ or $y^n(= \epsilon_2)$ can be modeled as a Markovian model. It is to be noted that the high-dimensional mapping is performed in a subtle Bayesian framework and the mapped input-output relation cannot be directly envisioned. With first order Markov dynamics assumption and considering process noise $\vartheta^n_{(\cdot)}$ the equivalent form of Eq. (1 and 2) for input strain $u^n(= \epsilon_1)$ at location 1 can be expressed as

$$
\begin{aligned}
(5) \qquad X^n(m) &= g^n_u(X^n(m-1), d^n; A^n_u) + \vartheta^n_X(m) \\
(6) \qquad u^n(m) &= h^n_u(X^n(m), d^n; B^n_u) + \vartheta^n_u(m)
\end{aligned}
$$

and for output strain $y^n(= \epsilon_2)$ at location 2 can be expressed as

$$
\begin{aligned}
(7) \qquad X^n(m) &= g^n_y(X^n(m-1), d^n; A^n_y) + \vartheta^n_X(m) \\
(8) \qquad y^n(m) &= h^n_y(X^n(m), d^n; B^n_y) + \vartheta^n_y(m)
\end{aligned}
$$

where $X^n(m) \in R^d$ denotes the d-dimensional latent coordinates at m^{th} lag coefficient of the nth damage level. Also $\vartheta^n_{(\cdot)}$ is the zero-mean, white Gaussian process noise, $g^n_{(\cdot)}$ and $h^n_{(\cdot)}$ are nonlinear mapping functions parameterized by $A^n_{(\cdot)}$ and $B^n_{(\cdot)}$ respectively. The nonlinear mapping functions $g^n_{(\cdot)}$ and $h^n_{(\cdot)}$ at n^{th} damage level can be expressed as linear combination of basis functions ϕ and ψ and is expressed as below.

(9)
$$g^n_{(\cdot)}(X^n(m-1), d^n; A^n) = \sum_i A^n_i \phi^n_i$$

(10)
$$h^n_{(\cdot)}(X^n(m-1), d^n; B^n) = \sum_j B^n_j \psi^n_j$$

where $A^n = \{A^n_1, A^n_2, \ldots, A^n_M\}$ and $B^n = \{B^n_1, B^n_2, \ldots, B^n_M\}$ are weights. In order to fit the parameters of this model to training data, one must select an appropriate number of basis function i.e., in other way to select the proper order of the system. One must ensure that there is enough data to constrain the shape of the basis functions. Ensuring enough data and finding the proper order of the system can be very difficult in practice. However, from a Bayesian perspective, the specific form of mapping function $g^n_{(\cdot)}$ and $h^n_{(\cdot)}$ are incidental and therefore should be marginalized out. Following GP regression modeling [4, 9, 17], the discrete short term time-series measurements at n^{th} damage level can be modeled for the input strain $u^n(= \epsilon_1)$ as

(11) $$f(\mathbf{u}^n|\{\mathbf{X}^n_m\}_{m=1,\ldots,M}) = \frac{1}{(2\pi)^{M/2}\sqrt{det\mathbf{K}^n_u}}exp[-\frac{1}{2}(\mathbf{u}^n - \boldsymbol{\mu}_u)^T(\mathbf{K}^n_u)^{-1}(\mathbf{u}^n - \boldsymbol{\mu}_u)]$$

Similarly for output strain $y^n(= \epsilon_2)$ as

(12) $$f(\mathbf{y}^n|\{\mathbf{X}^n_m\}_{m=1,\ldots,M}) = \frac{1}{(2\pi)^{M/2}\sqrt{det\mathbf{K}^n_y}}exp[-\frac{1}{2}(\mathbf{u}^n - \boldsymbol{\mu}_y)^T(\mathbf{K}^n_y)^{-1}(\mathbf{u}^n - \boldsymbol{\mu}_y)]$$

where $\mathbf{u}^n = [u^n(m = 1), u^n(m = 2), \ldots, u^n(m = M)]$ or $\mathbf{u}^n = [\epsilon^n_1(m = 1), \epsilon^n_1(m = 2), \ldots, \epsilon^n_1(m = M)]$ is the short term input time series at n^{th} damage level. Similarly $\mathbf{y}^n = [y^n(m = 1), y^n(m = 2), \ldots, y^n(m = M)]$ or $\mathbf{y}^n = [\epsilon^n_2(m = 1), \epsilon^n_2(m = 2), \ldots, \epsilon^n_2(m = M)]$ is the short term output time series at n^{th} damage level. In addition K^n_u and K^n_y are $M \times M$ kernel matrices with respect to $X \rightarrow u$ and $X \rightarrow y$ mappings. The elements of kernel matrix can be found using assumed kernel functions. There are different types of kernel functions (e.g., constant kernel, Radial basis kernel, Multilayer perceptron kernel, etc.) [21]. From the modeling point of view the choice of kernel should best suit our data. In the present application Multilayer perceptron (MLP) kernel is used. It is to be noted that the MLP kernel is a non-stationary kernel and is assumed that the MLP kernel will be more suitable to model a non-stationary fatigue damage process, particularly if the damage state does not remain constant between $n = N$ and $n = N + \Delta N$ fatigue cycles. The elements of nth damage level kernel matrix can be found using MLP kernel function as shown below.

$$
\begin{aligned}
(K^n_{(\cdot)})_{i,j} &= k(\mathbf{X}_i, \mathbf{X}_j) = k(\Phi(\mathbf{U}_i), \Phi(\mathbf{U}_j)) \\
&= (\theta^n_{(\cdot)})_p Sin^{-1}\frac{\mathbf{U}^T_i(\theta^n_{(\cdot)})_w\mathbf{U}_j}{\sqrt{(\mathbf{U}^T_i(\theta^n_{(\cdot)})_w\mathbf{U}_i + 1)(\mathbf{U}^T_j(\theta^n_{(\cdot)})_w\mathbf{U}_j + 1)}} + (\theta^n_{(\cdot)})_\vartheta
\end{aligned}
$$

(13)

In Eq. (13), $(\theta^n_{(\cdot)})_p$, $(\theta^n_{(\cdot)})_w$, $(\theta^n_{(\cdot)})_\vartheta$ are the process, width and noise hyperparameters, respectively. There are two sets of hyperparameters: $\Theta^n_u = \{(\theta^n_u)_p, (\theta^n_u)_w, (\theta^n_u)_b, (\theta^n_u)_\vartheta\}$ for $X \rightarrow u$ mapping and $\Theta^n_y = \{(\theta^n_y)_p, (\theta^n_y)_w, (\theta^n_y)_b, (\theta^n_y)_\vartheta\}$ for $X \rightarrow y$ mapping and can be found by minimizing the following two negative log-likelihood functions.

$$(14) \qquad \Gamma_u^n = -\frac{1}{2}logdet\mathbf{K}_u^n - \frac{1}{2}(\mathbf{u}^n)^T(\mathbf{K}_u^n)^{-1}\mathbf{u}^n - \frac{M}{2}log2\pi$$

$$(15) \qquad \Gamma_y^n = -\frac{1}{2}logdet\mathbf{K}_y^n - \frac{1}{2}(\mathbf{y}^n)^T(\mathbf{K}_y^n)^{-1}\mathbf{y}^n - \frac{M}{2}log2\pi$$

2.2. Time-series fatigue damage state estimation. Above subsection discussed how to estimate the nonlinear dynamic model for any individual damage instance. This subsection discusses how to estimate the time-series damage states at individual damage instances. The estimation of dynamic model for any individual damage instance is a fast scale dynamical system identification problem. Compared to this, the time-series damage state estimation for entire fatigue life is a slow scale dynamical system identification problem. The process for time-series damage state estimation for the entire fatigue life is discussed below.

2.2.1. *Reference model estimation.* Given the reference environmental condition $U^0(m) = \{L^n(m), T^n(m), H^n(m)\}$ and input strain $u^0(=\epsilon_1^0)$ and output strain $y^0(=\epsilon_2^0)$ the reference nonlinear dynamic models $H_{U \to u}^0$ (to estimate Θ_u^0) and $H_{U \to y}^0$ (to estimate Θ_y^0) can be estimated by minimizing the respective reference condition negative log-likelihood functions given below.

$$(16) \qquad \Gamma_u^0 = -\frac{1}{2}log\ det\ \mathbf{K}_u^0 - \frac{1}{2}(\mathbf{u}^0)^T(\mathbf{K}_u^0)^{-1}\mathbf{u}^0 - \frac{M}{2}log2\pi$$

$$(17) \qquad \Gamma_y^0 = -\frac{1}{2}log\ det\ \mathbf{K}_y^0 - \frac{1}{2}(\mathbf{y}^0)^T(\mathbf{K}_y^0)^{-1}\mathbf{y}^0 - \frac{M}{2}log2\pi$$

In Eq. (16 and 17) the kernel matrix can be written in the functional form as

$$(18) \qquad \mathbf{K}_u^0 = \Omega(\mathbf{U}^0, u^0, k(\mathbf{X}_i, \mathbf{X}_j))$$

$$(19) \qquad \mathbf{K}_y^0 = \Omega(\mathbf{U}^0, y^0, k(\mathbf{X}_i, \mathbf{X}_j))$$

In Eq. (18 and 19) $k(\mathbf{X}_i, \mathbf{X}_j)$ is the assumed kernel function given in Eq. (13).

2.2.2. *Current damage level dynamic strain mapping.* Once the reference $(n = 0)$ level dynamic models $H_{U \to u}^0$ and $H_{U \to y}^0$ are estimated, for a new environmental conditions $\mathbf{U}^n = [U^n(m = 1), U^n(m = 2), \ldots, U^n(m = M)]^T$, the corresponding input strain $\mathbf{u}_p^n = [u_p^n(m = 1), u_p^n(m = 2), \ldots, u_p^n(m = M)]$ and output strain $\mathbf{y}_p^n = [y_p^n(m = 1), y_p^n(m = 2), \ldots, y_p^n(m = M)]$ can be predicted using the probability density function (pdf)given below.

$$(20) \qquad f(u_m^n|\Theta_u^0, \mathbf{K}_u^0, \mathbf{X}^n(m)) = \mathbf{N}\left[\mu_u(m), \sigma_u^2(m)\right]; m = 1, 2, \ldots, M$$

$$(21) \qquad f(y_m^n|\Theta_y^0, \mathbf{K}_y^0, \mathbf{X}^n(m)) = \mathbf{N}\left[\mu_y(m), \sigma_y^2(m)\right]; m = 1, 2, \ldots, M$$

where $\mathbf{X}^n(m) = \Phi(\mathbf{U}^n(m))$ is the high dimensional transformation of the new environmental input $\mathbf{U}^n(m)$ at n^{th} damage level. $\mathbf{N}$ represents the Gaussian distribution with mean

$$(22) \qquad \mu_u(m) = (\mathbf{k}_u^n(m))^T(\mathbf{K}_u^0)^{-1}\mathbf{u}^0\ ;\ m = 1, 2, \ldots, M$$

$$(23) \qquad \mu_y(m) = (\mathbf{k}_y^n(m))^T(\mathbf{K}_y^0)^{-1}\mathbf{y}^0\ ;\ m = 1, 2, \ldots, M$$

and variance

$$(24) \qquad \sigma_u^2(m) = \kappa_u^n(m) - (\mathbf{k}_u^n(m))^T(\mathbf{K}_u^0)^{-1}\mathbf{u}^0\ ;\ m = 1, 2, \ldots, M$$

$$(25) \qquad \sigma_y^2(m) = \kappa_y^n(m) - (\mathbf{k}_y^n(m))^T(\mathbf{K}_y^0)^{-1}\mathbf{y}^0\ ;\ m = 1, 2, \ldots, M$$

where $(M \times M)$ $\mathbf{K}^0_{(\cdot)}$ matrix, $(M \times 1)$ $\mathbf{k}^n_{(\cdot)}(m)$ vector and scalar $\kappa^n_{(\cdot)}(m)$ can be found using the larger $(M + 1 \times M + 1)$ partitioned matrix given below.

$$(26) \qquad \mathbf{K}^n_{(\cdot)}(m) = \begin{bmatrix} \mathbf{K}^0_{(\cdot)} & \mathbf{k}^n_{(\cdot)}(m) \\ (\mathbf{k}^n_{(\cdot)}(m))^T & \kappa^n_{(\cdot)}(m) \end{bmatrix} \; ; \; m = 1, 2, \ldots, M$$

Following Eq. (20 - 26) the predicted input strain at n^{th} damage level can be rewritten as $\mathbf{u}^n_p = [\mu^n_u(m = 1), \mu^n_u(m = 2), \ldots, \mu^n_u(m = M)]$ and output strain given as $\mathbf{y}^n_p = [\mu^n_y(m = 1), \mu^n_y(m = 2), \ldots, \mu^n_y(m = M)]$

2.2.3. *Current damage level error signal estimation.* Due to damage the nonlinear dynamical model given by Eq. (1 - 4) will change from one damage level to other damage level. However if the dynamic model parameter is kept fixed (as reference model parameter), the nth damage level predicted input strain $\mathbf{u}^n_p$ will not be same as the actual input strain $\mathbf{u}^n_a$ (measured in real-time from the corresponding sensors). Similar is the case for the predicted output strain $\mathbf{y}^n_p$. The error in predicted signal and actual signal at a given damage level can be a measure of the damage state at that damage level. The error signals $e^n_{(\cdot)}$ for both the input and output strain are given as

$$(27) \qquad e^n_u(m) = u^n_a(m) - u^n_p(m) \; ; \; m = 1, 2, \ldots, M$$
$$(28) \qquad e^n_y(m) = y^n_a(m) - y^n_p(m) \; ; \; m = 1, 2, \ldots, M$$

2.2.4. *Time-series damage state estimation.* Once the error signal with respect to the input and output strain are estimated the corresponding scalar damage index a^n at n^{th} damage level can be estimated using either of the following two damage index formulations. The expression for root mean square error based damage index is given as,

$$(29) \qquad a^n = \sqrt{\frac{1}{M} \sum_{m=1}^{m=M} [e^n_{(u \; or \; y)}(m)]^2} \; ; \; n = 1, 2, \ldots, N - \Delta N, N, N + \Delta N$$

where $e^n_{(\cdot)}(m)$ are the error signals as described in Eq. (27) and (28). This damage index formulation can depend on either the input error signal $(e^n_u(m))$ or the output error signal $(e^n_y(m))$. A second damage index formulation using both the input error signal $(e^n_u(m))$ and output error signal $(e^n_y(m))$ is described below. This damage index is based on our previous work[11] for online damage state estimation under constant amplitude fatigue loading in which, the damage index was formulated by directly correlating the input dynamic strain $(u^n(m) = \epsilon^n_1(m))$ with the corresponding output dynamic strain $(y^n(m) = \epsilon^n_2(m))$. In contrast to the present random loading case, the damage index is formulated by correlating the input error signal $(e^n_u(m))$ with output error signal $(e^n_y(m))$. The expression for the developed damage index is given below.

$$(30) \qquad a^n = \sqrt{\frac{\sum_{m=-M}^{m=M} (\gamma^n_{e_u e_y}(m) - \gamma^0_{e_u e_y}(m))^2}{\sum_{m=-M}^{m=M} (\gamma^0_{e_u e_y}(m))^2}} \; ; \; n = 1, 2, \ldots, N - \Delta N, N, N + \Delta N$$

where $\gamma^n_{e_u e_y}(m)$ is the mth lagged cross correlation coefficient between the error signal e_u and e_y. Superscripts $'n'$ and $'0'$, represent the nth and reference state damage levels, respectively. It is to be noted that the reference damage level does not have to be the healthy condition of a structure.

3. Results and Discussion

Validation of the numerical model described in the previous section is a complex task. The "described" numerical prediction must to be validated by experimental results. Towards the validation goal, a fatigue test was conducted under biaxial random load. Using the real-time test data, damage states were estimated at different fatigue damage levels. The details of the numerical exercise are discussed below.

3.1. **Fatigue experiment and data collection.** The experimental validation of the developed model was carried out using data from fatigue tests performed on an Al-2024-T351 cruciform specimen under biaxial random loading. The cruciform specimen loaded in an MTS biaxial fatigue test frame can be seen in Figure 3. The specimen was instrumented with strain gauges as shown in Figure 4A. Two strain gauge rosettes are placed at different locations to measure the input strain ϵ_1 and the output strain ϵ_2, respectively. In the present case, the individual strain gauges of the 3-axis rosette gauges are aligned along the X-axis, 45° to X-axis and Y-axis of the MTS frame, respectively. Although in a typical application it is not necessary to follow any particular alignment direction, for better correlation of sensor signals the input and output rosettes should be placed parallel to each other. Figure 4A also shows the healthy condition of the cruciform specimen, while Figure 4B shows its failed condition. To accelerate the crack propagation, a 1.5 mm EDM notch was made at the bottom right boundary of the central hole. Also, to further accelerate the crack growth, the specimen was fatigued under constant cycle loading (maximum load of 4800 lbf and minimum load of 480 lbf), to achieve a visible crack (in front of the EDM notch) length of 1-2 mm. Then the specimen was tested under biaxial random loading. From the finite element stress analysis results the yield load was found to be 7200 lbf. Based on this limiting yield load, random load patterns were generated. The original patterns were generated using MATLAB and then coded to the MTS controller. Typical 1 block (equivalent of 300 cycles) of original random load pattern is shown in Figure 5. In the present random loading case all the blocks are non-repetitive which means that each block is different from every other block. The random loading patterns were generated using MATLAB while maintaining the maximum load limitat equal to 80 percent of the yield load and minimum load limited to 6.6 percent of the yield load. For every random loading block strain gauge signals and MTS load cell signals were acquired using a 48-channel NI-PXI data acquisition system (Figure 3). During testing both the X and Y-axis load frame actuators were programmed to operate at the same phase with a cyclic frequency of 10Hz. However, to capture high-frequency damage signatures, the strain gauge signals were acquired at a 1000 Hz sampling frequency. In order to maintain same data length, the MTS X and Y-axis load cell signals were also acquired with the same sampling frequency. The load cell and strain gauge measurements for a typical (healthy or reference state) random load block is shown in Figure 6. Part of the data based on Figure 6 is shown in Figure 7 in a magnified form. It is to be noted that, in the present work, the GP state estimation approach only requires relative strain signals at different locations. Hence it was not necessary to acquire the true or absolute strain field of the structure and so the strain gauges were not calibrated. Figures 6 and 7 show the uncalibrated strain signals.

3.2. **Time-series damage state estimation.** An approach for estimating the current damage level (n^{th} damage level) input and output error signals was presented in theoretical section. The estimated error signals at different damage levels can be used to estimate the corresponding scalar damage states. The individual damage states can be estimated using either the root mean square error (RMSE) based damage index or the correlation analysis (CRA) based damage index given in Eq. (29) and Eq. (30). The normalized damage states estimated using root mean square error based damage index formulation is shown in Figure 8. The normalized damage states estimated using both input strain error signal as well as output strain error signal are shown. In addition, the figure shows the normalized crack length estimated from the visual image captured by a high resolution camera. It is to be noted that the random loading fatigue test was started with a pre-cracked (with 1.5 mm
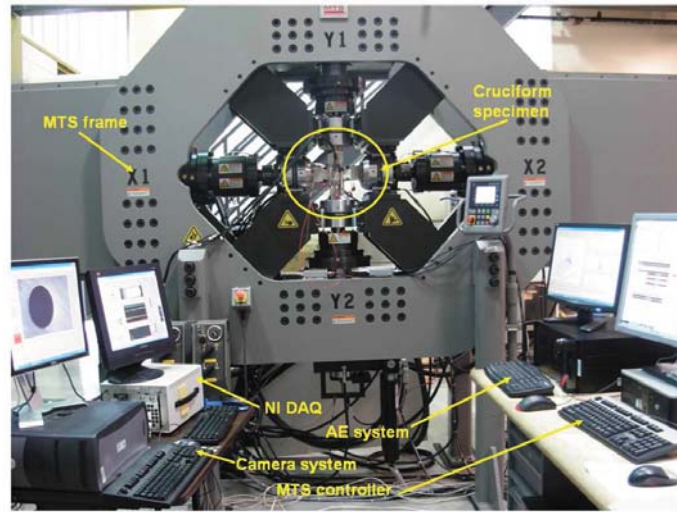
FIGURE 3. Biaxial testing experimental setup. The figure shows a MTS biaxial/torsion frame mounted with an Al-2024 cruciform specimen.
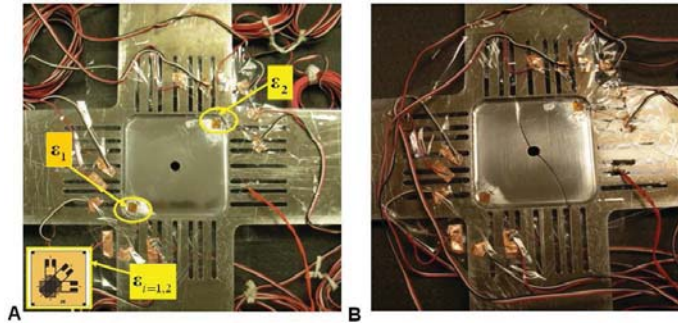

FIGURE 4. A) Instrumented Al-2024 undamaged cruciform specimen. Two 3-axis rosette strain gauges were placed on both sides of the crack path to monitor dynamic strain. B) Damaged Al-2024 cruciform specimen.

crack in front of 1.5mm EDM notch) specimen. In the pre-cracked specimen a stable crack grew up to the bottom wedge boundary resulting in a total length of 43.1 mm (Figure 4B) then a second crack started at the top edge of the central hole. The stable crack (equivalent to 43.1 mm crack length) reached the bottom boundary of the central wedge in approximately 380680 fatigue cycles. The second crack growth was unstable and grew to a total length of 28 mm (Figure 4B) within 3320 fatigue cycles. Figure 8 shows only the time-series damage state estimation in the stable crack growth regime. For proper comparison the estimated damage states from both proposed SHM model and visual images are normalized against their maximum value. From Figure 8 it can be seen that the estimated damage states using the input strain error signal follows a similar trend as that of estimated damage states using the output strain error signal. However, it can be seen that except during the final failure regime, the estimated damage states do not follow the trend of normalized visual measurements. A similar trend in estimated damage states only during the final failure regime is also observed by other works [22, 8]). However it is clear that it is better to identify the fault trend long before the final failure regime. The correlation analysis based damage state estimation given by Eq. (30) can be used to improve the prediction horizon. The estimated damage states
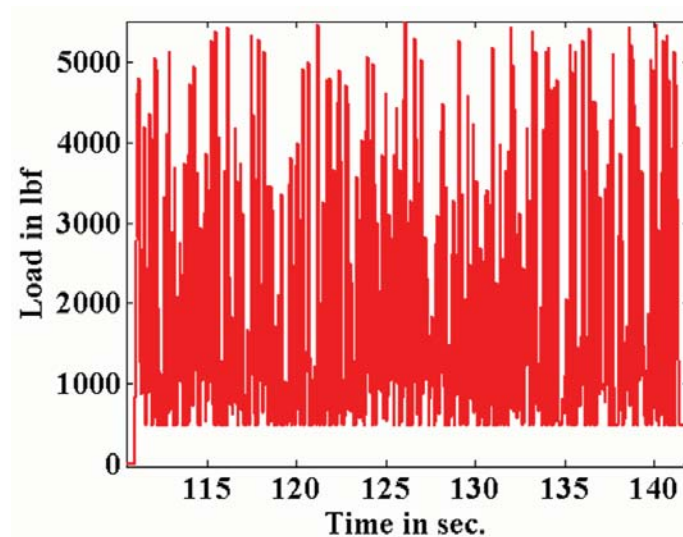
FIGURE 5. 1-block of random load. Each block of random load is equivalent to 300 fatigue cycles. Individual random load blocks were generated using MATLAB random number generator.
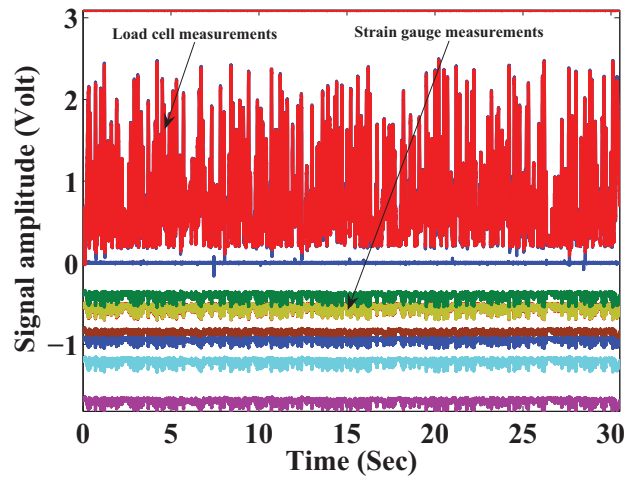

FIGURE 6. Plot of the raw sensor signals collected at a typical (reference or healthy state) damage level. The plot shows both load cell (from MTS frame X and Y-axis load cells) measurements and signals from different strain gauges.

using Eq. (30) is shown in Figure 9. It can be seen that there is a very good correlation between predicted damage states and normalized visual measurements over almost the entire stage-II and III damage growth regime.
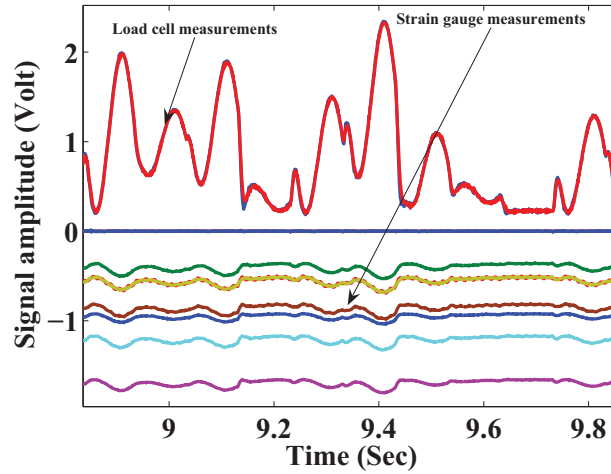
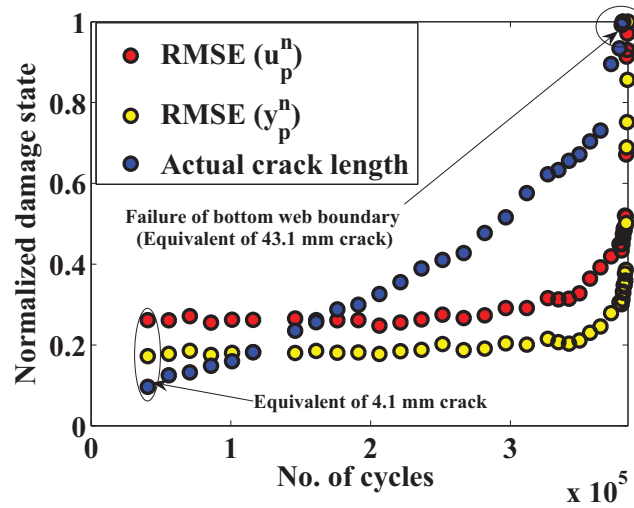FIGURE 7. Magnified version of the time-series signals shown in Figure 6

FIGURE 8. Time-series damage states using root mean square error (rmse) based damage index

4. CONCLUSION

A passive sensing based SHM technique has been developed to estimate the real-time fatigue damage state of complex structures subjected to random fatigue loading. The methodology uses the predicted and actual dynamic strains at two different locations in the structure. Ideally these locations are positioned on opposite sides of the damage path. First, individual reference condition dynamic models are estimated by mapping the reference condition applied load with the reference condition estimated equivalent strain. The reference condition equivalent strains are estimated using the measurements from 3-axis strain gauge rosettes placed at the corresponding locations. The reference condition dynamic models are estimated using Bayesian Gaussian process approach. Once the reference models are estimated, the dynamic strains are predicted for any applied load at any given instant of time using these models. The predicted strains are compared with the actual
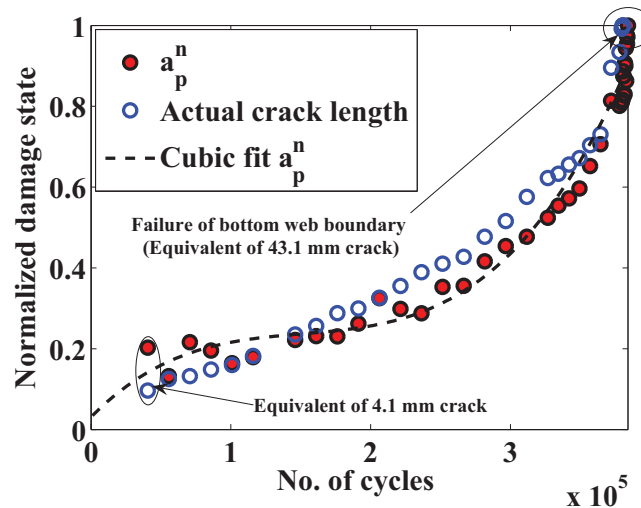
FIGURE 9. Time-series damage states using correlation analysis (CRA) based damage index

sensor measurements to estimate the corresponding error signals. Finally the error signals at the two locations are correlated to estimate the corresponding fatigue damage state. The approach is demonstrated for time-series damage state estimation of an Al-2024 cruciform test structure subjected to biaxial random fatigue loading. To verify the accuracy of the approach, the predicted damage states are compared with the actual damage states estimated using visual images. The comparison shows a good correlation between the predicted and actual time-series damage states almost over the entire stage-II and III crack growth regime. Further improvement of the prediction accuracy can be achieved by using global optimization and advanced signal processing techniques.

ACKNOWLEDGMENTS

REFERENCES

[1] A. Cuc, V. Giurgiutiu, S. Joshi, and T. Z. Structural health monitoring with piezoelectric wafer active sensors for space applications. *AIAA Journal*, 45(12), 2007.
[2] C. Farrar, K. Worden, M. Todd, G. Park, J. Nichols, D. Adams, M. Bement, and K. Farinholt. *Nonlinear System Identification for Damage Detection*. Los Alamos Report No. LA-14353, Los Alamos National Laboratory, USA, 2007.
[3] M. L. Fugate, H. Sohn, and C. R. Farrar. Vibration-based damage detection using statistical process control. *Mechanical Systems and Signal Processing*, 15(4):707 – 721, 2001.
[4] M. N. Gibbs. *Bayesian Gaussian Processes for Regression and Classification*. PhD Thesis, University of Cambridge, University of Cambridge, U.K., 1997.
[5] S. Gupta and A. Ray. Real-time fatigue life estimation in mechanical structures. *Journal of Meas. Sci. Technol*, 18:1947 – 1957, 2007.
[6] N. Iyer, S. Sarkar, R. Merrill, and N. Phan. Aircraft life management using crack initiation and crack growth models - p-3c aircraft experience. *International Journal of Fatigue*, 29:1584 – 1607, 2007.
[7] A. Jardine, D. Lin, and D. Banjevic. A review on machinery diagnostics and prognostics implementing condition-based maintenance. *Mechanical Systems and Signal Processing*, 20:1483 – 1510, 2006.
[8] D. G. Lewicki, P. J. Dempsey, G. F. Heath, and P. Shanthakumaran. *Gear Fault Detection Effectiveness As Applied To Tooth Surface Pitting Fatigue Damage*. U.S. Army research laboratory report, Number ARL-RP-0247, Army research laboratory, USA, 2009.

[9] D. MacKay. *Information Theory, Inference, and Learning Algorithms.* Cambridge university press, U.K., 2003.

[10] S. Mohanty, A. Chattopadhyay, and P. Peralta. Adaptive residual useful life estimation of a structural hotspot. *Journal of Intelligent Material Systems and Structures, (special issues on SHM, on-line version available)*, 21:321 – 335, 2010.

[11] S. Mohanty, A. Chattopadhyay, J. Wei, and P. Peralta. Real time damage state estimation and condition based residual useful life estimation of a metallic specimen under biaxial loading. *Structural Durability and Health Monitoring Journal (Invited paper), Accepted and on-line version available*, 5(1):33 – 55, 2009.

[12] S. Mohanty, A. Chattopadhyay, J. Wei, and P. Peralta. Unsupervised time-series damage state estimation of complex structure using ultrasound broadband based active sensing. *Structural Durability and Health Monitoring Journal (on-line version will shortly available)*, 130(1):101 – 124, 2010.

[13] T. Ogunfunmi. *Adaptive Nonlinear system identification: The Volterra and Winer model approaches.* Springer Publishing, New York, 2007.

[14] G. Park, C. A. Rutherford, and et. all. High-frequency response functions for composite plate monitoring with ultrasonic validation. *AIAA Journal*, 43:2431 – 2437, 2003.

[15] G. Park, H. Sohn, C. R. Farrar, and D. J. Inman. Overview of piezoelectric impedance-based health monitoring and path forward. *Shock and Vibration Digest*, 35(6):451 – 463, 2003.

[16] H. Qiua, J. Leea, J. Linb, and G. Yu. Wavelet filter-based weak signature detection method and its application on rolling element bearing prognostics. *Journal of Sound and Vibration*, 289:1066 – 1090, 2006.

[17] C. Rasmussen and C. Williams. *Gaussian Processes for Machine Learning.* MIT Press, Cambridge, MA, 2006.

[18] S. Salamone, I. Bartoli, F. Lanza di Scalea, and S. Coccia. Guided-wave health monitoring of aircraft composite panels under changing temperature. *Journal of Intelligent Materials Systems and Structures*, 20:1079 – 1090, 2009.

[19] H. Sohn and C. R. Farrar. Damage diagnosis using time series analysis of vibration signals. *Journal of Smart Materials and Structures*, 10:446 – 451, 2001.

[20] H. Sohn, C. R. Farrar, F. M. Hemez, D. D. Shunk, D. W. Stinemates, and B. R. Nadler. *A Review of Structural Health Monitoring Literature from 1996 to 2001.* Los Alamos National Laboratory report LA-13976-MS, Los Alamos National Laboratory, USA, 2004.

[21] C. K. I. Williams. *Computing with infinite networks, Advances in Neural Information Processing Systems, Vol. 9.* MIT Press, Cambridge, MA, 1997.

[22] T. Williams, X. Ribadeneira, S. Billington, and T. Kurfess. Rolling element bearing diagnostics in run-to-failure lifetime testing. *Mechanical Systems and Signal Processing*, 15(5):979 – 993, 2001.

[23] M. Witczak. *Modelling and estimation strategy for fault diagnosis of non-linear systems: From analytical to soft computing approaches.* Springer-Verlag, Berlin Heidelberg, 2007.